Dielectric microwave characterizations of (Ba,Sr)TiO3 film deposited on high resistivity silicon substrate : analysis by two-dimensional tangential finite element method

Freddy Ponchel, J. Midy, Jean-François Legier, Caroline Soyer, Denis Remiens, T. Lasri, G. Gueguan

Dielectric microwave characterizations of $(Ba, Sr)TiO_3$ film deposited on high resistivity silicon substrate: Analysis by two-dimensional tangential finite element method

Cite as: J. Appl. Phys. **107**, 054112 (2010); https://doi.org/10.1063/1.3309423
Submitted: 05 October 2009 • Accepted: 09 January 2010 • Published Online: 15 March 2010

F. Ponchel, J. Midy, J. F. Legier, et al.

Dielectric microwave characterizations of $(Ba,Sr)TiO_3$ film deposited on high resistivity silicon substrate: Analysis by two-dimensional tangential finite element method

F. Ponchel,[1,a] J. Midy,[1] J. F. Legier,[1] C. Soyer,[1] D. Rémiens,[1] T. Lasri,[1] and G. Guéguan[2]
[1]*Institute of Electronics, Microelectronics, and Nanotechnology (IEMN), UMR CNRS 8520, Université des Sciences et Technologies de Lille, BP 60069, 59652 Villeneuve d'Ascq Cedex, France*
[2]*STMicroelectronics, SAS 16, rue Pierre et Marie Curie, BP 7155, 37071 Tours, France*

(Received 5 October 2009; accepted 9 January 2010; published online 15 March 2010)

$(Ba,Sr)TiO_3$ (BST) thin films were deposited on high resistivity silicon substrates by *in situ* rf magnetron sputtering. A buffer layer was used to improve the cristallinity of the films, the composition was fixed to Ba/Sr=30/70. The relative permittivity and the losses were measured up to 60 GHz using coplanar strip lines. The dispersion of the permittivity and the losses has been determined with a home made numerical code based on finite elements: ELFI. We show that, with the measurements of the scattering parameters coupled with ELFI, it is possible to know the BST complex permittivity over a very broad frequency band. The BST films deposited by *in situ* (700 °C) present excellent properties between 1 to 60 GHz. The relative permittivity is in the order of 270 and the losses are very small 0.09 at 60 GHz. These structures BST/silicon high resistivity show good potentialities for devices microwaves applications which need future integration in a silicon environment. © *2010 American Institute of Physics*. [doi:10.1063/1.3309423]

I. INTRODUCTION

Ferroelectric thin films, such as $(Ba,Sr)TiO_3$ (BST), are being widely investigated for applications in integrated dynamic random access memory cells, decoupling capacitors, and microwave tunable devices, including tunable mixers, delay lines, filters, and phase shifters for steerable antennas.[1–3] As $Pb(Zr,Ti)O_3$ for piezoelectric micro/nanosystems applications,[4] BST has become the leading materials system for these devices due to its high dielectric response and its tunability near the ferroelectric phase transformation temperature. The transition temperature (Tc) can be controlled via adjusting composition; for example, the Tc of bulk $Ba_{0.60}Sr0_{0.40}TiO_3$ (60/40) is just below room temperature.[5] By adjusting the composition of BST films, the Tc and, hence, the dielectric properties and its tunability can be tailored. Therefore, several compositions of BST thin films have been studied in great detail for use in tunable microwave devices employing a variety of different fabrication methods (sol gel, pulsed laser deposition, and sputtering)[6–9] and substrates. Many types of substrates have been used: MgO and sapphire.[10,11] These substrates are "ideal" in that sense they are very well adapted, in terms of parameters cell to obtain epitaxial growth of BST (identical lattice parameters) and of losses at high frequency; therefore the microwaves measurements are "easy" since the losses induced by the substrate are very low. The use of Silicon is more complicated to extract the properties of the films since the substrate has a strong influence on the behavior of the total structure. But since the main objective for BST devices applications is the integration with silicon for integrated circuit (IC) it is imperative to optimize the BST deposition directly onto silicon. For the microwave's applications, it is clear that BST films must combined high permittivity with low dielectric loss on silicon. The limitation in practical device applications of ferroelectric materials at microwaves frequency is their dielectric losses. Researchers found that BST films with low losses and high dielectric breakdown fields can be grown using magnetron sputter deposition with judiciously chosen process parameters. In particular, *in situ* deposition at high temperature seems to be the best process deposition to obtain BST film which presents low losses. On the other hand, it was found that doping of low loss oxides, such as MgO, ZrO_2, TiO_2, and Al_2O_3 into ferroelectric material, is an effective way to reduce the loss tangent.[12–14] The effect generally observed is an improvement of the dielectric losses in comparison to undoped case but in contrary the relative permittivity decreases. So, it is very difficult to find a good compromise between low loss and high permittivity at microwaves frequency with BST ferroelectric materials.

There are a limited number of papers which try to understand or to analyze the mechanisms at the origin of the BST dielectric losses behavior at microwaves frequency: Debye mechanism [presence of charged defects, nanopolar regions in the material as in lead magnesium niobate-lead titanate (PMN-PT)], interaction with phonons.[15,16] It seems very important to analyze the dispersion frequency of the relative permittivity and the dielectric losses of BST films in a wide range of frequency. In our work, we have focused on the characterizations of BST films deposited on silicon high resistivity (SiHr) substrates between 1 to 60 GHz at room temperature. The growth of BST onto SiHr is a necessary technological step in running in IC and it is imperative to qualify completely and "properly" this structure. By properly, we mean that we want absolutely distinguish the losses due to the metallic electrodes (coplanar strip lines), the losses

[a]Author to whom correspondence should be addressed. Electronic mail: freddy.ponchel@univ-lille1.fr.

TABLE I. Typical sputtering conditions of BST film with a buffer layer on SiHr substrate.

	Buffer layer	Main layer
Target composition (Ba/Sr)	30/70	30/70
rf power	70 W	70 W
Gas composition	100% Ar	100% Ar
Sputtering time	50 min	720 min
	Temperature	
Increasing temperature slope	10 °C/min	20 °C/min
Deposition temperature	800 °C	700 °C
Decreasing temperature slope	20 °C/min	20 °C/min

induced by the SiHr from the losses of BST films. Our approach is consequently based on a complete determination of the scattering [S] parameters of monolayered and bilayered structures where the experimental results are coupled to a numerical homemade software (ELFI). Hence we extract the main properties of BST films in a wide range of frequency at room temperature. This work at ambient temperature, is a necessary preliminary step to the understanding of losses mechanism at lower temperature.

II. EXPERIMENTS AND MEASUREMENTS

A. The BST films

The BST films, with composition 30/70, were deposited on SiHr substrates; we have chosen this composition because it is a good compromise between high dielectric constant, low loss and high tunability. The targets are composed from $BaTiO_3$ and $SrTiO_3$ powders mixed together in stoechiometric quantity (Ba/Sr=30/70) and uniaxially cold pressed. The films were deposited by *in situ* rf magnetron sputtering, more precisely the substrate temperature is fixed to 700 °C. We have made many experiments to determine this optimized temperature. The growth conditions are given in Table I; the sputtering gas is pure Ar. As the BST was directly deposited onto silicon, the crystallization, as it is well known, was poor. In order to improve this property, we have used a buffer layer. Many types of buffer layers have been selected in the past to optimize the BST crystallization. In this work, in order to develop a simple process we have decided to depose a buffer layer of the same composition of the "active" film but at higher growth temperature. The details of the deposition run are described Fig. 1; the buffer layer was deposited at 800 °C during 50 min which corresponds to a

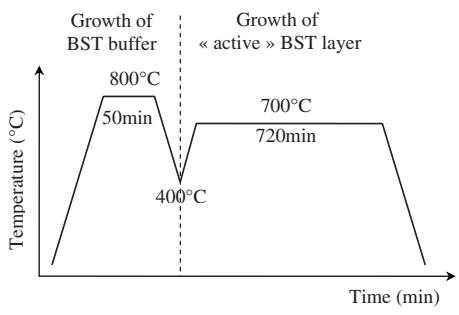

FIG. 1. Substrate temperature during sputtering process.

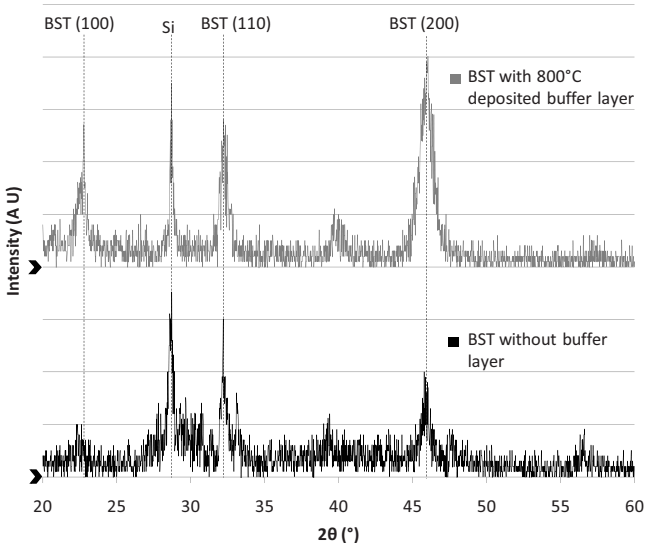

FIG. 2. X-ray diffraction patterns of BST films. Gray line: crystallization of BST deposited on SiHr at 700 °C with buffer layer deposited at 800 °C. Black line: crystallization without buffer layer.

film thickness of 100 nm. Directly on Si, it is necessary to depose at very high temperature in order to obtain a crystallization of the BST film; this is the reason why we have chosen 800 °C for the deposition of the buffer layer. After a decrease in the substrate temperature, without the plasma, at a temperature to 400 °C (to relax the stresses in the film), the growth of the active layer begin at 700 °C and during 720 min which corresponds to a film thickness of 1.3 μm. For the active layer, we have made some deposition at 800 °C but no improvement of the BST crystallization has been observed so we decide to operate at 700 °C. No post annealing treatment was made after deposition. A typical x rays diffraction obtained with these conditions is shown Fig. 2. Pure perovskite phase was observed, i.e., we remarked no second phase. We do not also note any interdiffusion between the buffer and the "active" layer. The buffer layer permits to enhance the crystallization and acts like a starter. The orientation given by the buffer layer is the one of the active layer. Hence, the (100) orientation of BST is more intense with the presence of the buffer layer. But even with the buffer layer, the film was polycrystalline without a preferred orientation; the "total" film thickness (buffer layer +active layer) is in the order of 1.3 μm. For the microwaves measurements, we have used coplanar strip lines and it is very important for the quality of the measurements to have good film thickness homogeneity (1.3 ± 0.1 μm on a sample of 6.25 cm^2). Therefore we have optimized the substrate position in relation to the species flux emitted from the target (the substrates are in off-axis position). The composition of the film is valued with Rutherford backscattering spectrometry (RBS). RBS spectra are acquired at a backscattering angle of 160° and an appropriate grazing angle. The sample is oriented perpendicularly to the incident He^{2+} ion beam which has energy of 2.275 MeV. The Ba/Sr ratio of the film is similar to that of the target.

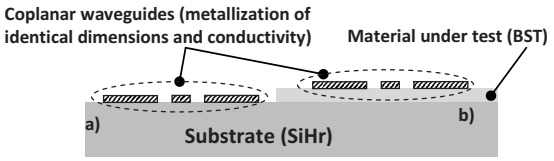

FIG. 3. Scheme of the cross-section of a tested structure: (a) coplanar strip electrodes directly onto SiHr, (b) coplanar strip electrodes on BST previously deposited on the same SiHr substrate.

B. Protocol overview for measurement and extraction of BST thin film complex permittivity

We can now focus on microwave measurements and dielectric properties of the complete structure: SiHr/BST/coplanar strip lines. The protocol we have developed is structured around these following steps. In order to collect pertinent information in microwave range, we decided to pattern metallic electrodes on the SiHr substrates and on the SiHr/BST structures. From an excitation point of view, the electrodes have the well known coplanar topology. It is the most convenient and versatile structure when commercial on-wafer probing system are used such as "cascade coplanar microtech probe station." So, we need consequently three metallic strips, two of them being devoted to ground whereas the central conductor concerns the signal in the well known ground-signal-ground probe excitation.[17] To avoid spurious behaviors and to ensure only one mode of propagation, all the dimensions of the metallic electrodes and dielectric substrate are optimized.[18,19] These gold electrodes are realized by optical lithography, evaporation, and lift-off process onto SiHr substrates [Fig. 3(a)] and onto the BST film which has been deposited on the same silicon wafer [Fig. 3(b)]. The structures previously described are obviously different, but at this step, we can hope that we have patterned a couple of coplanar lines with identical metallization and especially with the same conductivity because they are processed simultaneously. The objective is now to determine with a maximum of accuracy the conductivity of the metallization and the complex permittivity of the SiHr substrate [Fig. 3(a)] because there is dispersion on manufactured SiHr specifications and some variations on the dimensions (thickness of metallization and width of the lines) of coplanar lines. Once this task is done, we naturally focused on the characterization of the two layered structure [Fig. 3(b)] and so on the BST film. From a practical point of view, the above pertinent information we get are the [S] parameters. In our protocol, they are intermediate ones from which we extract the complex propagation constant with an appropriate de-embedding home made software.[20,21] The real and imaginary components of this complex value are respectively dedicated to the attenuation and to the phase constant of the mode which propagates. From a numerical point of view, we have implemented a second home made numerical software based on a two dimensional tangential vector finite element method named "ELFI."[22–24] All widths and thicknesses are precisely measured and act as data entries. Real and imaginary parts of dielectric or magnetic constant of any layer are changeable parameters. Finally, the unknown complex dielectric permittivity is adjusted for each frequency, in such a way that the calculated complex propagation constant matched the measured complex one.

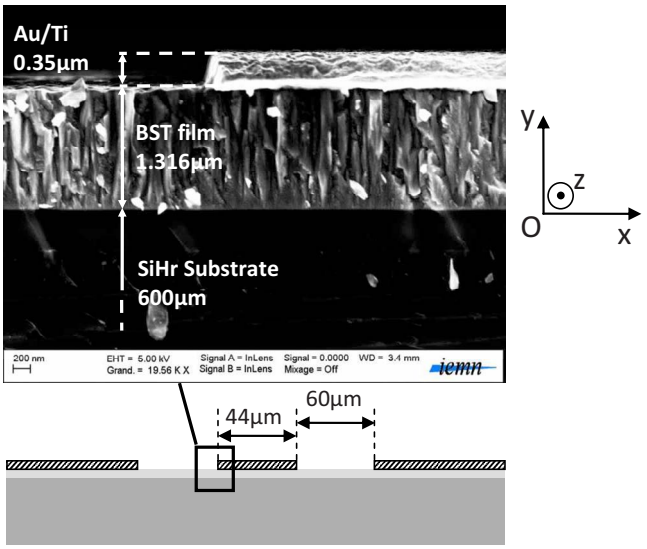

FIG. 4. (Color online) SEM view of a part of the tested coplanar structure and cross-section dimensions. We have magnified the corner of the central conductor to get information on shape and thickness of conductor and BST layer.

1. Dimensions, scanning electron microscope (SEM) view and cross-section drawing for finite element numerical study

We remember some dimensions about one typical cross-section of the tested structure realized on a 600 μm thickness wafer of SiHr. In Fig. 4, we focus on one interesting part of the structure. Indeed, we have made a zoom on the corner metallization and the BST film. As we can see, the central conductor made of gold and titanium laid on 1.31 μm of BST. We have noticed a very small deviation of these values from the nominal ones in the transverse plane xOy (Fig. 4). In the Oz direction of propagation, there is no more than 3% relative variations in the transversal dimensions linked to the length of the electrodes which varies from 5 to 15 mm. These observations show that we have a very reproducible technological process and allow us to implement these data entries in the drawing of the multilayered coplanar structure for finite element study. Figure 5 shows a typical mesh where about 4500 triangles are used to discretize the whole cross-section including the BST layer, the coplanar electrodes and the SiHr substrate. We use the same mesh to treat the structure without BST. Indeed, in order to get reliable informations, we keep identical discretization and consequently the same number of triangles to describe the structures with and without BST film. This means also, that the area named «layer» on Fig. 5 is made equally well of SiHr or BST according to the study of basic electrodes deposited on single SiHr substrate or double layer made of BST on SiHr. We must also note that we mesh the electrodes cross-section with one layer of triangles in accordance with the skin effect. The skin depth is of 0.36 μm at 60 GHz for an average conductivity of $33\times10^{+6}$ S/m.[25,26] This value is

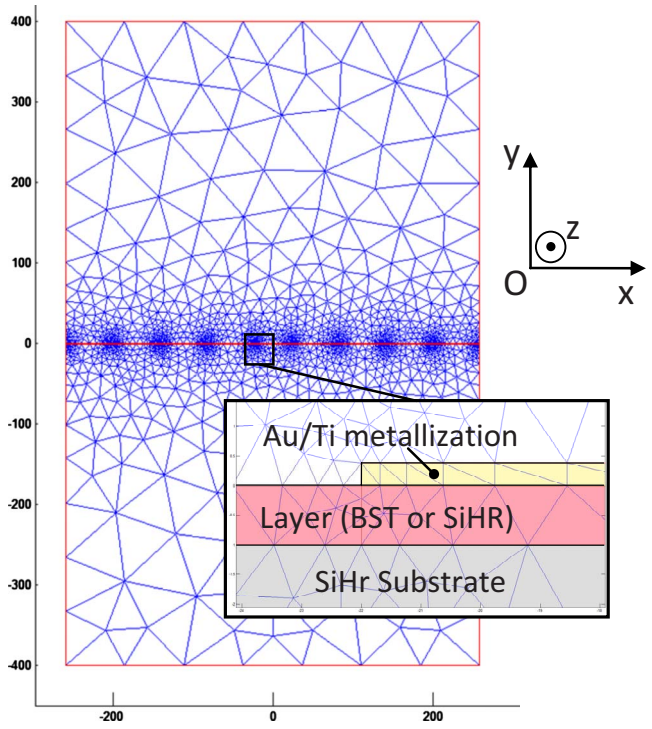

FIG. 5. (Color online) Typical mesh of the whole cross-section whose dimension are defined in micrometer. We zoom on the corner area of the central gold conductor to show the discretization in the thin layer of metallization and BST.

those of a single metallization equivalent to the double layer Au/Ti of 0.35 μm thickness.

2. Conductivity of the electrodes and complex permittivity determination of the SiHr wafer

All our measurements are performed, in ambient temperature, with an Agilent vectorial network analyzer E8361A coupled to a Cascade Microtech probe station. The [S] parameters are measured for structures depicted Figs. 3 and 4 in the 1 to 60 GHz frequency band for the fundamental mode.

We focus now, as it is needed in our protocol, on the single SiHr substrate. Our main objective is to determine the conductivity of the patterning electrodes and their impact on the measured attenuation of the SiHr coplanar structure. On Fig. 6, the solid lines concerns only the results deduced from the de-embedding of the [S] parameters measurements. These results illustrate the frequency behavior of the attenuation constant in neper per meter. All the dotted lines in Fig. 6 must be assigned to numerical calculations when dielectric losses of the SiHr substrate are voluntarily omitted. This means that the imaginary part of the complex dielectric permittivity of SiHr is ignored so as to determine the conductivity of the coplanar electrodes which produce the same losses as those measured. This approach is reliable and valid at low frequency when dielectric losses are negligible.[27,28] We found typically, at 0.1 GHz, $\sigma=33.1\times10^{+6}$ S/m for the conductivity of the gold metallization and $\varepsilon_r=11.15$ for the relative dielectric permittivity of the substrate. These data being constant in the whole frequency band, we observed rationally some discrepancies between measured and calculated values. This is especially visible after 20 GHz when dielectric losses mechanisms become significant. In order to point out the sensitivity of the attenuation to a small variation in the conductivity of the electrodes, we have tuned the nominal value of $\sigma=33.1\times10^{+6}$ S/m from $\sigma=32\ 10^{+6}$ to $\sigma=34\times10^{+6}$ S/m. As we can see, it has a significant impact on the attenuation even at low frequencies. So, in such a context, it is not possible to find an erroneous value of the conductivity. As this value is now considered as a constant data in our software, the complex permittivity of SiHr is automatically modified to match numerical with measured complex propagation constant values. This procedure gives, on Fig. 7, the frequency behavior of the complex permittivity $\varepsilon^*=\varepsilon'-j\varepsilon''$ of the SiHr substrate and of the loss tangent known as $\tan(\delta)=\varepsilon''/\varepsilon'$.

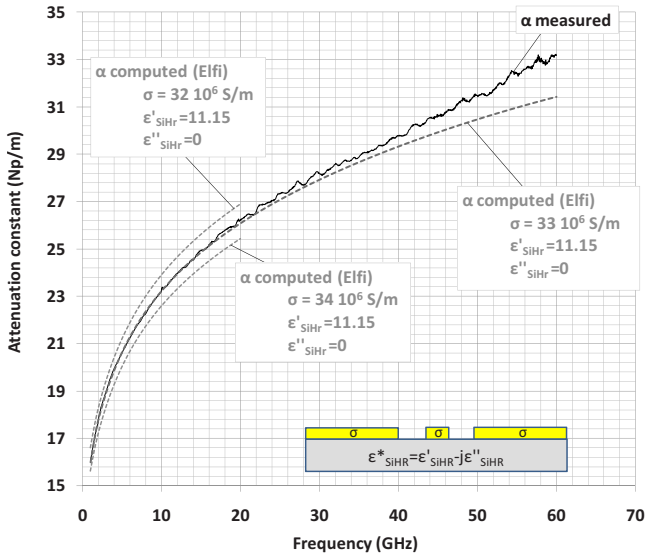

FIG. 6. (Color online) Frequency behavior of the attenuation constant of coplanar guide realized on SiHr substrate. The solid line represents the experimental values of the attenuation due to dielectric and metallic losses. It is extracted from 401 [S] parameters measure points. The dashed lines are only linked to calculated metallic losses with our software for three values of the conductivity of the metallic strips. In this case, the dielectric losses of SiHr are voluntarily ignored.

3. Complex permittivity determination of the BST layer

The physical parameters reported in Fig. 7 as well as the conductivity $\sigma=33.1\times10^{+6}$ S/m act now as data in our home made numerical software. For each frequency, the unknown complex permittivity of the BST film laid on the SiHr layer are deduced thanks to the same matching propagation constant procedure. So, we naturally obtained Fig. 8 the two components of the complex dielectric permittivity of the BST material as well its loss tangent named $\tan(\delta)$. A quick look on this figure gives nominal values of the relative dielectric permittivity $\varepsilon'=290$ at 1 GHz, $\varepsilon'=285$ at 10 GHz, and $\varepsilon'=270$ at 60 GHz. We observe a low decrease in the permittivity of BST with frequency; the dispersion in this frequencies range is weak. The loss tangent stays small even at high frequency: $\tan(\delta)=0.007$, 0.03, and 0.09 at 1, 10, and 60 GHz, respectively.

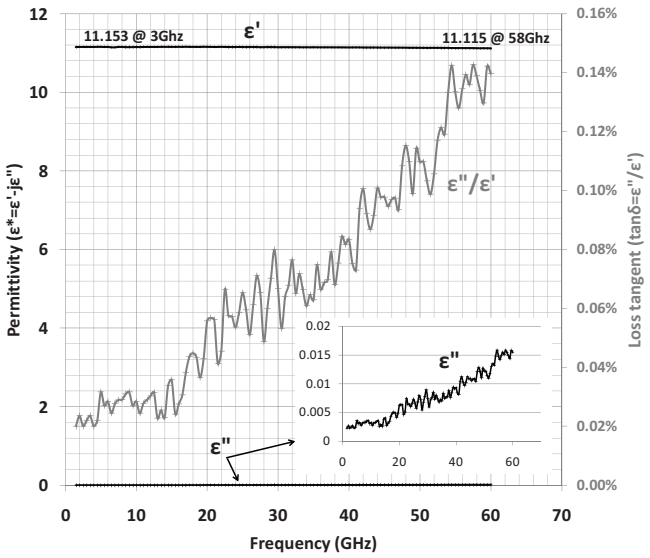

FIG. 7. Frequency behavior of the complex permittivity ($\varepsilon^*=\varepsilon'-j\varepsilon''$) and loss tangent [$\tan(\delta)=\varepsilon''/\varepsilon'$] of the SiHr substrate. We zoom on the imaginary part of complex permittivity (ε'') to give more details on its variation.

III. CONCLUSION

This paper presents the dielectric properties of BST films deposited on SiHr substrate in a large frequency range (1–60 GHz). In order to extract the influence of the substrate and the coplanar strip lines electrodes on the "real" dielectric properties of BST, we have defined a strict experimental protocol. The obtained results coupled with our numeric code (ELFI) permit to give a precise value of the permittivity and the loss factor of the BST films. A high accuracy degree has been reached because we have measured also precisely the resistivity of the metallic coplanar electrodes (Ti/Au) and the permittivity of the SiHr substrate. Even deposited directly on silicon, the film performance is very good: $\varepsilon'=270$ and $\tan(\delta)=0.09$ at 60 GHz. The introduction of the buffer layer improves the crystalline quality of the film. We have demonstrated the potentiality of the integration of BST with silicon substrate. Always with this experimental protocol and our numeric code the second step is now to determine the tunability of the structure.

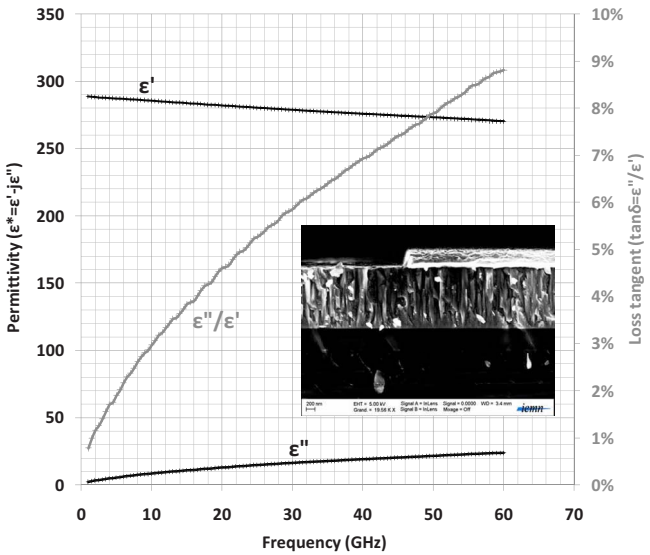

FIG. 8. (Color online) Real and imaginary part (black lines) of dielectric permittivity of a 1.31 μm thickness BST layer deposited on a 600 μm SiHr substrate vs frequency and corresponding loss tangent (gray line). These values have been extracted and computed from 401 [S] parameters measure points with fixed conductivity for metallization ($\sigma=33.1\times10^{+6}$ S/m) and known frequency complex permittivity dependance of SiHr previously shown in Fig. 7.

[1]W. K. Simon, E. K. Akdogan, and A. Safari, Appl. Phys. Lett. **89**, 022902 (2006).
[2]K. P. Jayadevan, C. Y. Liu, and T. Y. Tseng, J. Am. Ceram. Soc. **88**, 2456 (2005).
[3]C. Berbecaru, H. V. Alexandru, C. Porosnicu, A. Velea, A. Ioachim, L. Nedelcu, and M. Toacsan, Thin Solid Films **516**, 8210 (2008).
[4]P. Muralt, J. Am. Ceram. Soc. **91**, 1385 (2008).
[5]A. Kholkin, A. Wu, and P. M. Vilarinho Recent Res. Dev. Mater. Sci. **5**, 1 (2004).
[6]D. R. Patil, S. A. Lokare, R. S. Devan, S. S. Chougule, C. M. Kanamadi, Y. D. Kolekar, and B. K. Chougule, Mater. Chem. Phys. **104**, 254 (2007).
[7]H.-S. Kim, H.-G. Kim, II-D. Kim, K.-B. Kim, and J.-C. Lee, Appl. Phys. Lett. **87**, 212903 (2005).
[8]L. A. Knauss, J. M. Pond, J. S. Horwitz, D. B. Chrisey, C. H. Mueller, and R. Treece Appl. Phys. Lett. **69**, 25 (1996).
[9]C. L. Chen, H. H. Feng, Z. Zhang, A. Brazdeikis, Z. J. Huang, W. K. Chu, C. W. Chu, F. A. Miranda, F. W. Van Keuls, R. R. Romanofsky, and Y. Liou, Appl. Phys. Lett. **75**, 412 (1999).
[10]H. Li, J. Finder, Y. Liang, R. Gregory, and W. Qin, Appl. Phys. Lett. **87**, 072905 (2005).
[11]Y. Gim, T. Hudson, Y. Fan, C. Kwon, A. T. Findikoglu, B. J. Gibbons, B. H. Park, and Q. X. Jia, Appl. Phys. Lett. **77**, 1200 (2000).
[12]J. Im, O. Auciello, P. K. Baumann, S. K. Streiffer, D. Y. Kaufman, and A. R. Krauss, Appl. Phys. Lett. **76**, 625 (2000).
[13]K. T. Kang, M.-H. Lim, H.-G. Kim, Y. W. Choi, H. L. Tuller, I.-D. Kim, and J.-M. Hong, Appl. Phys. Lett. **87**, 242908 (2005).
[14]M. S. Tsai, S. C. Sun, and T. Y. Tseng, J. Appl. Phys., **82**, 3482 (1997).
[15]N. Setter, D. Damjanovic, L. Eng, G. Fox, S. Gevorgian, S. Hong, A. Kingon, H. Kohlstedt, N. Y. Park, G. B. Stephenson, I. Stolitchnov, A. K. Taganstev, D. V. Taylor, T. Yamada, and S. Streiffer, J. Appl. Phys. **100**, 051606 (2006).
[16]A. K. Tagantsev, V. O. Sherman, K. F. Astafiev, J. Venkatesh, and N. Setter, J. Electroceram. **11**, 5 (2003).
[17]S. A. Watenberg, IEEE Trans. Microwave Theory Tech. **51**, 1413 (2003).
[18]Y. D. Lin and J. W. Sheen, IEEE MTT-S Int. Microwave Symp. Dig., **3**, 1701 (1994).
[19]F. Schnieder, T. Tischler, and W. Heinrich, IEEE Trans. Microwave Theory Tech. **51**, 137 (2003).
[20]J. Grzyb and G. Troster, IEEE Microw. Wirel. Compon. Lett. **14**, 213 (2004).
[21]N. J. Farich and P. M. Asbeck, AEU, Int. J. Electron. Commun. **63**, 287 (2008).
[22]J. Lee, D. Sun, and Z. J. Cendes, IEEE Trans. Microwave Theory Tech. **39**, 1262 (1991).
[23]F. Ponchel, Ph.D. dissertation, University of LILLE, 2007.
[24]F. Ponchel, J. F. Legier, E. Paleczny, C. Séguinot, and D. Deschacht, "Proximity effect of neighbour victim lossy interconnects on a single attacker and vice versa," in IEEE International Symposium on Integrated Circuits (ISIC 2007), Singapore, 2007, p. 406 (available on IEEE Xplore 2.0: Integrated Circuits).
[25]R. Faradji-dana and Y. L. Chow, IEE Proc. Microwaves, Antennas Propag. **37**, 133 (1990).
[26]P. Waldow and I. Wolf, IEEE Trans. Microwave Theory Tech. **33**, 1076 (1985).
[27]W. Heinrich, IEEE Trans. Microwave Theory Tech. **41**, 45 (1993).
[28]R. E. Collin, *Field Theory of Guided Waves* (McGraw-Hill, New York, (1960).